

Measurement Based Evaluation of Interference Alignment on the Vienna MIMO Testbed

Martin Mayer, Gerald Artner, Gabor Hannak, Martin Lerch and Maxime Guillaud

Institute of Telecommunications

Vienna University of Technology, Austria

Gusshausstrasse 25/389, A-1040 Vienna, Austria

Email: { mmayer, gartner, ghannak, mlerch }@nt.tuwien.ac.at, guillaud@tuwien.ac.at

Abstract—Interference Alignment (IA) is a linear precoding scheme for the K -user interference channel with high signal to noise ratio. Ideally, interference is completely suppressed and each user is able to achieve half of the single-user multiple-input multiple-output (MIMO) degrees of freedom. We use the Vienna MIMO testbed to evaluate the feasibility of IA in realtime¹, in a heterogeneous outdoor to indoor and indoor to indoor scenario representative of an urban scenario. We evaluate the accuracy of alignment and provide benchmarks for typical delays in such a setup.

I. INTRODUCTION

With decreasing cell size and increasing number of users, interference has become the main limiting factor for high data rates in modern wireless telecommunication systems. Using multiple-input multiple-output (MIMO) transmission and coordinated base stations, the transmit signals can be precoded to mitigate interference at the receiver. One of such precoding schemes is Interference Alignment (IA) [1], where the precoders are chosen such that the interfering signals align in an interference subspace at the receiver. A linear filter can then be applied on the received signal so that the desired signal is projected onto an interference free subspace. It is theoretically known that IA works best at high signal to noise ratio (SNR), but the use of IA over physical channels and the impairments due to real equipment received little attention until recently.

Emulation of IA with measured channels was performed in [2]. IA was emulated for three users with two antennas per transmitter and receiver and one datastream per user, denoted² as $(2 \times 2, 1)^3$. The same setup was used to compare IA with time division multiple access (TDMA) and Interference Avoidance in an in- and outdoor environment [3]. IA was measured on a testbed in a $(2 \times 2, 1)^3$ indoor environment in [4], where the feasibility of IA in realtime applications has been shown and IA was found to outperform TDMA in the high SNR regime. Channel estimation, filter calculation and signal generation were computed online within five seconds. The testbed from [4] was further used in [5] to show how imperfect channel state information (CSI) influences the degrees of freedom. A moveable testbed with a $(2 \times 2, 1)^3$ setup and a

¹Realtime here states that all processes involved in the interference alignment computations take place online during the measurement and do not exceed a certain amount of time as defined in Section IV-B.

²A system denoted $(M \times N, d)^K$ consists of K transmitter-receiver pairs, each transmitter transmitting d data streams over M antennas and each receiver receiving d data streams over N antennas.

shorter delay for signal calculation was reported in [6]. Indoor measurements of IA were compared to coordinated multi-point (CoMP) and TDMA.

In this paper we use the Vienna MIMO testbed (VMTB) [7] with two outdoor transmitters, one indoor transmitter and one indoor receiver with four antennas each. In contrast to the aforementioned results, our approach performs IA computations and feedback online in a real outdoor to indoor scenario. We investigate the practical implementation and performance of $(4 \times 4, 2)^3$ IA and give benchmarks for precoder update delays on our testbed.

The remainder of this paper is organized as follows. Section II introduces the channel and precoding model. In Section III-A we give an overview of our testbed and the used hardware, in Section III-B we describe the structure of the transmitted signals, in Section III-C we explain our method of channel estimation and in Section III-D we introduce the quantities of interest for performance evaluation. In Section IV, we show measurements of aligned signals (Section IV-A) and provide typical time delays on our testbed (Section IV-B). The results are finally summarized in Section V.

II. CHANNEL MODEL AND INTERFERENCE ALIGNMENT

Let us consider a $(M \times N, d)^K$ MIMO interference channel. It has been shown that if $M + N \geq d(K + 1)$, on each link half of the interference-free degrees of freedom can be attained using suitable linear pre-processing of the data at the transmitters and post-processing of the data at the receivers by using IA [8, 9].

Due to the orthogonality of orthogonal frequency division multiplexing (OFDM) transmission, the channels can be described subcarrier-wise. In the following, we consider only one subcarrier. The channels between transmitter j and receiver i are represented by the matrix $\mathbf{H}_{ij} \in \mathbb{C}^{N \times M}$, where $i, j \in \{1, \dots, K\}$.

Let us consider the truncated unitary precoding matrix $\mathbf{V}_j \in \mathbb{C}^{M \times d}$ at the j^{th} transmitter and the interference suppression matrix $\mathbf{U}_i \in \mathbb{C}^{N \times d}$ at the i^{th} receiver. With the transmit data stream $\mathbf{s}_j \in \mathbb{C}^d$ at transmitter j , the receive data stream $\mathbf{r}_i \in \mathbb{C}^d$ at receiver i with additive noise $\mathbf{n}_i \in \mathbb{C}^N$ is³

$$\mathbf{r}_i = \sum_{j=1}^K \mathbf{U}_i^H \mathbf{H}_{ij} \mathbf{V}_j \mathbf{s}_j + \mathbf{U}_i^H \mathbf{n}_i. \quad (1)$$

³The Hermitian adjoint operator $(\cdot)^H$ denotes the conjugate transpose.

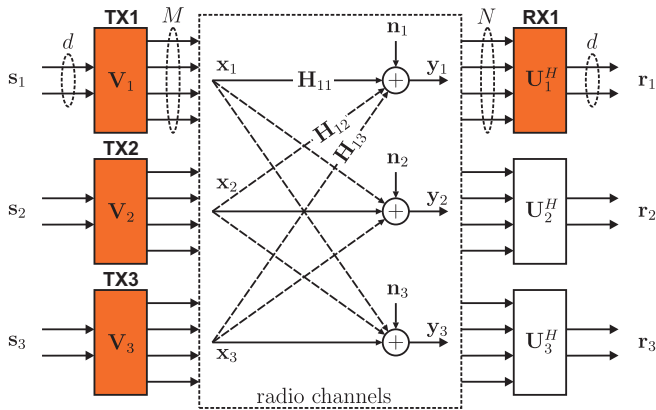


Fig. 1: IA in a $(4 \times 4, 2)^3$ OFDM system incorporating $K = 3$ users, $d = 2$ spatial streams and $M = N = 4$ antennas per user. The filled boxes indicate deployed stations available on VMTB.

According to [1], if

$$\mathbf{U}_i^H \mathbf{H}_{ij} \mathbf{V}_j = \mathbf{0}, \quad \forall j \neq i \quad (2)$$

and

$$\text{rank}(\mathbf{U}_i^H \mathbf{H}_{ii} \mathbf{V}_i) = d, \quad (3)$$

interference is aligned and \mathbf{r}_i contains information only about the data stream s_i of its corresponding i^{th} transmitter: the transmission chain corresponds to a $d \times d$ MIMO channel with channel coefficients $\mathbf{U}_i^H \mathbf{H}_{ii} \mathbf{V}_i$. An iterative algorithm for computing the \mathbf{U}_i and \mathbf{V}_j matrices almost surely satisfying Equation (2) and Equation (3) has been proposed in [1]. For the $(4 \times 4, 2)^3$ case depicted in Figure 1 and considered in Section IV, and under perfect channel knowledge, the precoding and interference suppression matrices \mathbf{V}_j and \mathbf{U}_i can be calculated analytically from the channel matrices as in [8].

III. SYSTEM DESCRIPTION

A. Overview

The Vienna MIMO testbed (VMTB) in the setup considered here consists of two outdoor (rooftop) transmitter stations TX1 and TX2, one indoor transmitter station TX3 and one indoor receiver station RX1. Their locations are depicted in Figure 2. TX3 and RX1 are situated in adjacent rooms on the 5th floor of the Institute of Telecommunications, Vienna University of Technology. They are not within line-of-sight of each other.

Each node comprises a personal computer (PC) for controlling purposes, radio frequency (RF) hardware, a synchronization unit and an antenna setup with $M = N = 4$ antennas⁴. All PCs are connected via a dedicated fiber network which constitutes an almost ideal feedback link.

Each transmitter utilizes an Innovative Integration X5-TX FIFO digital to analog converter (DAC) card to generate transmit signals at intermediate frequency (IF) 70MHz,

⁴ Used antennas:

TX1, TX2: KATHREIN Scala Division XX-pol outdoor antenna (800 10543)
 TX3: 2 × KATHREIN Scala Division X-pol indoor antenna (800 10677) with horizontal spacing of 26.56cm
 RX1: 4 × custom built $\lambda/2$ dipole (2 vertical, 2 horizontal) in laptop shell

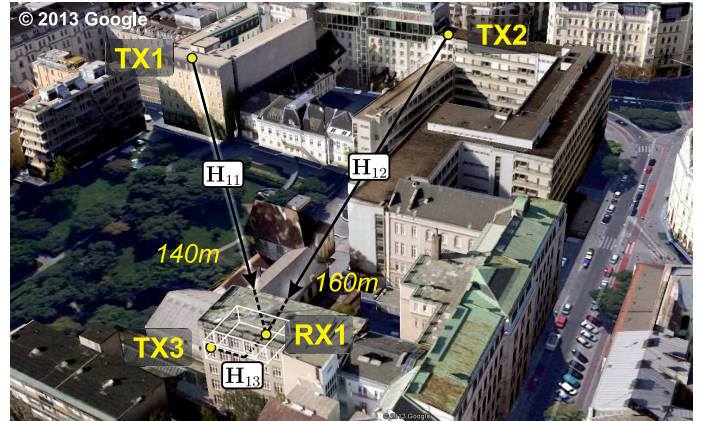


Fig. 2: Placement of transmitter and receiver stations. Antenna setups of transmitters 1 and 2 (TX1, TX2) are located outdoors, transmitter 3 (TX3) and receiver (RX1) indoors.

whereas the receiver utilizes an Innovative Integration X5-RX FIFO analog to digital converter (ADC) card to fetch the receive samples. These cards include four channels, work at a sampling frequency of 200MHz and have a resolution of 16 bit. At the transmitter, the RF hardware shifts the IF signals up to passband carrier frequency 2.503GHz and allows for transmitting at a transmit power of up to 35dBm. Synchronization is accomplished utilizing global positioning system (GPS) and a highly accurate rubidium clock at each node. The $N = 4$ receive antennas of RX1 are implemented in the shell of a laptop that resembles a possible user equipment. Additional information regarding our testbed hardware can be found in [7].

We use OFDM as modulation scheme, with a symbol duration of $66.6\mu\text{s}$, cyclic prefix duration of $8.8\mu\text{s}$ and a subcarrier spacing of 15kHz. Decoder complexity scales linearly with the number of subcarriers, but one subcarrier is sufficient to show the feasibility of IA. Therefore, only one subcarrier is considered in the sequel to ensure fast processing.

Our scenario coincides with the system described in Section II, depicted in Figure 1, up to the fact that we employ only one physical receiver station. The situation at RX2 and RX3 can be inferred from the observations at RX1, thanks to a symmetry argument. To establish $K = 3$ transmitter-receiver pairs and compensate for the two missing receivers, CSI $\hat{\mathbf{H}}_{2j}$ and $\hat{\mathbf{H}}_{3j}$ are randomly generated complex Gaussian matrices that do not change during one measurement cycle (see Section III-B), whereas the channel matrices to our physical receiver \mathbf{H}_{1j} are truly estimated by RX1, for all transmitters $j = \{1, 2, 3\}$. The estimation process that generates the CSI $\hat{\mathbf{H}}_{1j}$ in dependence of the true channel \mathbf{H}_{1j} is described in Section III-C.

The precoders fulfilling $\mathbf{U}_i^H \hat{\mathbf{H}}_{ij} \mathbf{V}_j = \mathbf{0}, \quad \forall j \neq i$, are then computed at RX1 and fed back to the respective transmitters.

B. Frame Structure

A measurement cycle entails a consecutive transmission of frames, each composed of a pilot preamble and an attached data sequence as depicted in Figure 3. After every transmission of a frame (indexed by l), RX1 computes the current CSI $\hat{\mathbf{H}}_{1j}^{(l)}$

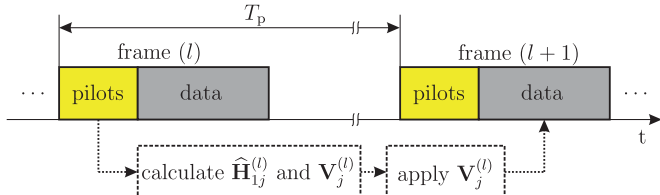


Fig. 3: Transmitted frames of transmitter j . Pilots are used to calculate CSI and the precoding matrix which is applied on the data of the next transmission.

and the corresponding precoders $\mathbf{V}_j^{(l)}$ for every transmitter $j = \{1, 2, 3\}$. The precoders are fed back to the transmitters via the dedicated fiber network. Each transmitter then applies its respective precoder on the $d = 2$ dimensional data stream $\mathbf{s}_j^{(l+1)}$ to generate the $M = 4$ dimensional transmit data signal

$$\mathbf{x}_j^{(l+1)} = \mathbf{V}_j^{(l)} \mathbf{s}_j^{(l+1)}. \quad (4)$$

Since precoders $\mathbf{V}_j^{(l)}$ computed from CSI $\widehat{\mathbf{H}}_{1j}^{(l)}$ are used for transmission of frame $l + 1$, IA might be impaired due to outdated CSI. We therefore aim for low processing time T_p between consecutive frames. In the following, we will omit the frame index $(\cdot)^{(l)}$ for simplicity.

The performance evaluation of the alignment (see Section III-D) is done offline.

C. Channel Estimation

The pilot sequences used for channel estimation are based on Zadoff-Chu sequences which are orthogonal to circularly shifted versions of themselves [10]. The utilized pilot sequence is shifted by one symbol for each antenna. In order to shorten them and thus decrease processing time T_p , each transmitter transmits its $M = 4$ pilot sequences on one of $K = 3$ adjacent subcarriers. The transmitters are hence orthogonal in frequency domain during pilot transmission. We assume that the three adjacent subcarriers undergo the same fading which was confirmed by measurements. This allows us to use the corresponding Zadoff-Chu sequence of length 4, in the form of the binary phase-shift keying (BPSK) sequence $\{1, 1, 1, -1\}$. Note that conversely to the pilot symbols, the data signals as in Equation (4) will still be transmitted on the same subcarrier.

The pilot sequences are optimized for least squares (LS) estimation. Each channel coefficient $(\mathbf{H}_{1j})_{nm}$ is estimated by correlating the sequence received at antenna n with the pilot sequence transmitted at antenna m of transmitter j .

D. IA Performance Evaluation

In the following, we declare TX1 our desired transmitter, whereas TX2 and TX3 are the interferers. The $N = 4$ dimensional signal at RX1 ($i = 1$) before interference suppression with \mathbf{U}_i^H is obtained as

$$\mathbf{y}_i = \sum_{j=1}^K \mathbf{H}_{ij} \mathbf{V}_j \mathbf{s}_j + \mathbf{n}_i, \quad (5)$$

where $\mathbf{n}_i \in \mathbb{C}^N$ contains the noise at receiver i which is assumed to be Gaussian i.i.d. with variance σ^2 . Assuming

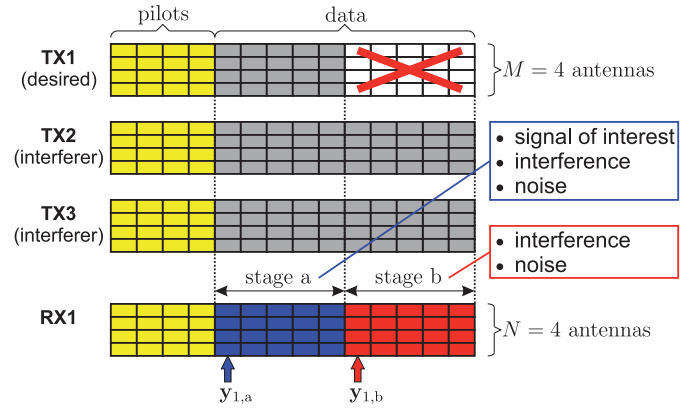


Fig. 4: Transmit signals and receive signal of one frame. We introduce two stages in order to calculate performance measures like MI.

Gaussian i.i.d. data symbols and letting P_j denote the transmit power, the corresponding covariance matrix

$$\begin{aligned} \mathbf{Q}_{\mathbf{y}_i} &= \mathbb{E}\{\mathbf{y}_i \mathbf{y}_i^H\} \\ &= \underbrace{P_i \mathbf{H}_{ii} \mathbf{V}_i \mathbf{V}_i^H \mathbf{H}_{ii}^H}_{\mathbf{Q}_S} + \underbrace{\sum_{\substack{j=1 \\ j \neq i}}^K P_j \mathbf{H}_{ij} \mathbf{V}_j \mathbf{V}_j^H \mathbf{H}_{ij}^H}_{\mathbf{Q}_I} + \underbrace{\mathbf{I}_N \sigma^2}_{\mathbf{Q}_N} \end{aligned} \quad (6)$$

decomposes into the respective covariance matrices of the signal of interest \mathbf{Q}_S , interference \mathbf{Q}_I and noise \mathbf{Q}_N . We are interested in the evaluation of the mutual information (MI) between \mathbf{s}_1 and \mathbf{y}_1 . Using [11]

$$\text{MI} = \log_2 \det(\mathbf{I}_N + \mathbf{Q}_S (\mathbf{Q}_I + \mathbf{Q}_N)^{-1}) = \log_2 \det(\mathbf{Q}_a \mathbf{Q}_b^{-1}) \quad (7)$$

with

$$\mathbf{Q}_a = \mathbb{E}\{\mathbf{y}_{1,a} \mathbf{y}_{1,a}^H\} = \mathbf{Q}_S + \mathbf{Q}_I + \mathbf{Q}_N, \quad (8)$$

$$\mathbf{Q}_b = \mathbb{E}\{\mathbf{y}_{1,b} \mathbf{y}_{1,b}^H\} = \mathbf{Q}_I + \mathbf{Q}_N, \quad (9)$$

where $\mathbf{y}_{1,a}$ and $\mathbf{y}_{1,b}$ denote the receive signal during *stage a* and *stage b* respectively, introduced to be able to estimate \mathbf{Q}_a and \mathbf{Q}_b directly as shown in Figure 4 and described in the following.

During *stage a*, all three transmitters transmit concurrently, we observe the $N = 4$ dimensional receive data signal $\mathbf{y}_{1,a}$ and compute its sample covariance matrix $\widehat{\mathbf{Q}}_a$. During *stage b*, the desired transmitter TX1 is turned off, we observe $\mathbf{y}_{1,b}$ and compute its sample covariance matrix $\widehat{\mathbf{Q}}_b$. $\widehat{\mathbf{Q}}_a$ and $\widehat{\mathbf{Q}}_b$ are used to estimate MI as

$$\widehat{\text{MI}} = \log_2 \det(\widehat{\mathbf{Q}}_a \widehat{\mathbf{Q}}_b^{-1}). \quad (10)$$

Furthermore, we want a measure for interference suppression. Let us introduce the unitary matrix

$$\mathbf{M} = [\mathbf{U}_i \ \mathbf{U}_i^\perp] \quad (11)$$

as concatenation of interference suppression matrix $\mathbf{U}_i \in \mathbb{C}^{N \times d}$ and a truncated unitary matrix $\mathbf{U}_i^\perp \in \mathbb{C}^{N \times N-d}$

spanning its orthogonal complement. Using Equation (9) and $\mathbf{M}\mathbf{M}^H = \mathbf{I}_N$, we obtain the eigenvalue decomposition

$$\mathbf{Q}_b = \underbrace{\mathbf{M} \begin{bmatrix} \mathbf{I}_d & \mathbf{0} \\ \mathbf{0} & \tilde{\mathbf{E}} \end{bmatrix}}_{\mathbf{E}} \underbrace{\begin{bmatrix} \mathbf{I}_d \sigma^2 & \mathbf{0} \\ \mathbf{0} & \mathbf{I}_{N-d} \sigma^2 + \tilde{\mathbf{\Lambda}} \end{bmatrix}}_{\mathbf{\Lambda}} \underbrace{\begin{bmatrix} \mathbf{I}_d & \mathbf{0} \\ \mathbf{0} & \tilde{\mathbf{E}} \end{bmatrix}^H}_{\mathbf{E}^H} \mathbf{M}^H \quad (12)$$

utilizing Equation (2), Equation (6), Equation (11) and the eigenvalue decomposition of the interference leakage covariance term

$$(\mathbf{U}_i^\perp)^H \mathbf{Q}_i \mathbf{U}_i^\perp = \tilde{\mathbf{E}} \tilde{\mathbf{\Lambda}} \tilde{\mathbf{E}}^H, \quad (13)$$

where $\tilde{\mathbf{E}} \in \mathbb{C}^{N-d \times N-d}$ is unitary and $\tilde{\mathbf{\Lambda}} = \text{diag}\{\tilde{\lambda}_1, \dots, \tilde{\lambda}_{N-d}\}$ contains the $N-d$ eigenvalues in non-decreasing order that correspond to the interference subspace.

Equation (12) shows that under perfect IA (Equation (2)), the eigenvectors in the last $N-d$ columns of \mathbf{E} span an $N-d$ dimensional subspace in which the interference is restricted. This implies that

$$\begin{aligned} \mathbf{\Lambda} &= \text{diag}\{\lambda_1, \dots, \lambda_N\} \\ &= \text{diag}\{\underbrace{\sigma^2, \dots, \sigma^2}_d, \underbrace{\tilde{\lambda}_1 + \sigma^2, \dots, \tilde{\lambda}_{N-d} + \sigma^2}_{N-d}\}, \end{aligned} \quad (14)$$

namely that the first d eigenvalues of \mathbf{Q}_b contain only the noise variance σ^2 . This is due to the fact that in *stage b*, no signal of interest is transmitted and we only receive noise and interference. If IA is impaired by inaccurate CSI, the first d eigenvalues will be larger than σ^2 due to leakage, meaning that we were not able to confine interference to its supposed $N-d$ dimensional subspace.

In our measurements, we encounter both additive noise and interference leakage due to imperfect CSI, therefore the first d eigenvalues will be lower bounded by the noise variance σ^2 .

We finally introduce the measure for interference suppression

$$I_{\text{supp}} = 10 \log_{10} \left(\frac{\lambda_{d+1}}{\lambda_d} \right) \text{dB} \stackrel{(d=2)}{=} 10 \log_{10} \left(\frac{\lambda_3}{\lambda_2} \right) \text{dB}, \quad (15)$$

the separation between smallest eigenvalue corresponding to the interference subspace (λ_{d+1}) and the largest eigenvalue corresponding to the presumably interference free subspace (λ_d).

IV. MEASUREMENT RESULTS

A. Results

In Figure 6, we summarize our measurement results which were obtained by one measurement cycle consisting of 1000 successive frame transmissions as described in Section III-B. Each frame consists of 4 pilot OFDM symbols per antenna and 10 data OFDM symbols per stream. The receiver position was fixed. Possible channel fluctuations are a result of moving scatterers (e.g. people, trees). The power contributions from all transmitters at the receiver (not shown here) are about equally strong (within ± 1.5 dB), meaning that each interfering signal is received as strong as the signal of interest.

Figure 6(a) shows measured eigenvalues from the sample covariance matrix $\hat{\mathbf{Q}}_b$ estimated during *stage b* of each frame (see Figure 4) where only interferers transmit data. Note that they were normalized so that the smallest eigenvalue corresponding to the interference subspace ($\lambda_{d+1} = \lambda_3$) lies at 0dB on average.

Figure 6(b) shows the empirical distribution of the normalized eigenvalues. We end up with a remarkable mean interference suppression of $\bar{I}_{\text{supp}} = 39$ dB, averaged over all transmissions.

Figure 6(c) shows the estimated mutual information as defined in Equation (10) vs. time over the 1000 transmissions. Figure 6(d) depicts the corresponding empirical distribution. The average mutual information amounts to $\bar{M}I = 28$ bit per channel use per subcarrier.

B. Latency Analysis

In Section III-B, we introduced the processing time T_p as the time between two successive frame transmissions including channel estimation and precoder update. The VMTB is quasi-realtime in the sense that we are able to guarantee that $T_p < 20$ ms. Reading from and writing to conventional hard disk drives (HDDs) takes a tremendous amount of time and introduces large delay jitters that counter realtime constraints. We mitigate this by using RAMDisk. The mean and standard deviation of T_p , denoted $(\mu_{T_p}, \sigma_{T_p})$, are reduced from (28ms, 10ms) with HDD to (17ms, 600 μ s) with RAMDisk.

Figure 5 illustrates the composition of the processing time. The time required to compute the IA solution is negligible compared to the other tasks, the largest delays come from synchronization, transmit signal generation and waiting for the received samples to be stored on the RAMDisk of the receiver.

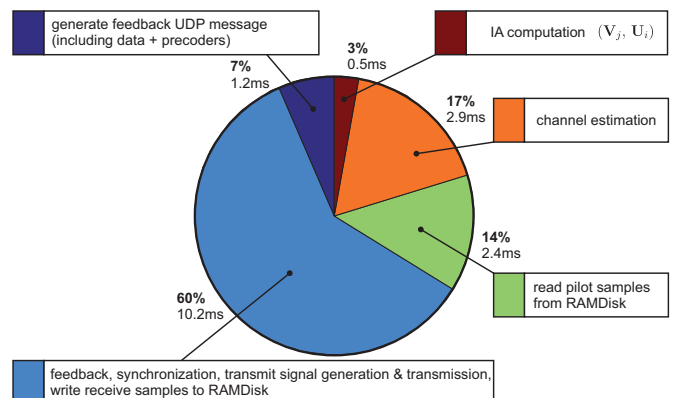


Fig. 5: Composition of processing time T_p .

V. CONCLUSION

We have first demonstrated the feasibility of IA on a realtime MIMO testbed using three transmitters with four antennas each. Transmitters were located both in- and outdoors to consider the future use of small cells. After giving an overview of our testbed, the structure of our signals and the used channel estimation scheme, we evaluated measurements of aligned transmissions. Furthermore we measured typical delays in such a setup.

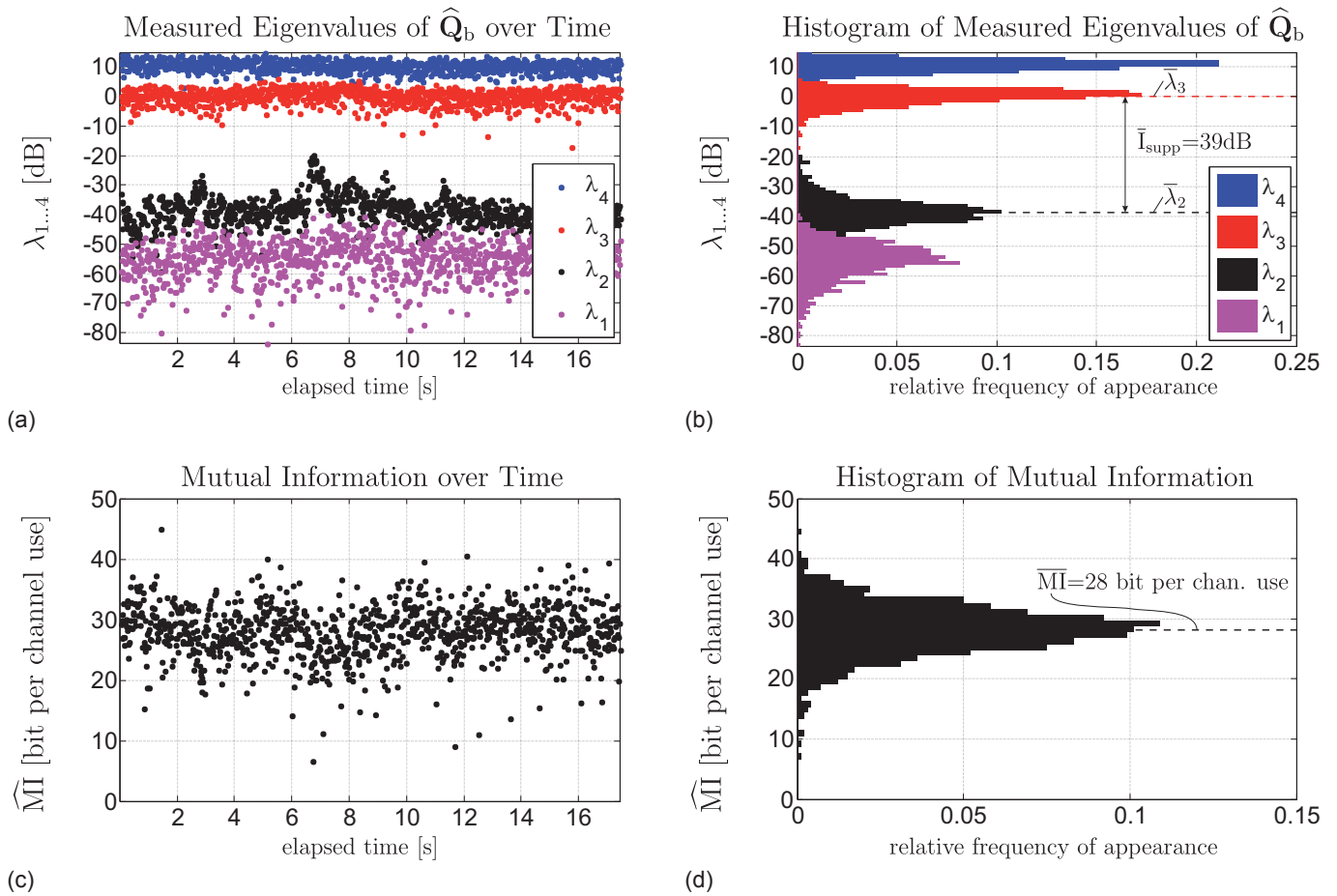


Fig. 6: Measurement results obtained by one measurement cycle including 1000 frame transmissions.

ACKNOWLEDGMENT

This work has been funded by the Christian Doppler Laboratory for Wireless Technologies for Sustainable Mobility, KATHREIN-Werke KG, and A1 Telekom Austria AG. The financial support by the Federal Ministry of Economy, Family and Youth and the National Foundation for Research, Technology and Development is gratefully acknowledged. This work was supported by the FP7 project HIATUS (grant #265578) of the European Commission and by the Austrian Science Fund (FWF) under project grants S10606 and S10611 within the National Research Network SISE.

REFERENCES

- [1] K. Gomadam, V.R. Cadambe and S.A. Jafar, "Approaching the Capacity of Wireless Networks through Distributed Interference Alignment", in *Global Telecommunication Conference (IEEE GLOBECOM)*, 2008
- [2] O. El Ayach, S.W. Peters and R.W. Heath Jr., "Real World Feasibility of Interference Alignment using MIMO-OFDM Channel Measurements", in *Military Communications Conference (MILCOM)*, 2009
- [3] O. El Ayach, S.W. Peters and R.W. Heath Jr., "The Feasibility of Interference Alignment over Measured MIMO-OFDM Channels", in *IEEE Transactions on Vehicular Technology*, Volume 59, Issue 9, Pages 4309-4321, November 2010
- [4] J.A. García-Naya, L. Castedo, Ó. González, D. Ramírez and I. Santamaria, "Experimental Validation of Interference Alignment Techniques using a Multiuser MIMO Testbed", in *International ITG Workshop on Smart Antennas (WSA)*, February 2011
- [5] J.A. García-Naya, L. Castedo, Ó. González, D. Ramírez and I. Santamaria, "Experimental Evaluation of Interference Alignment under Imperfect Channel State Information", in *19th European Signal Processing Conference (EUSIPCO)*, August 2011
- [6] P. Zetterberg and N.N. Moghadam, "An Experimental Investigation of SIMO, MIMO, Interference-Alignment (IA) and Coordinated Multi-Point (CoMP)", in *19th International Conference on Systems, Signals and Image Processing (IWSSIP)*, April 2012
- [7] S. Caban, C. Mehlführer, R. Langwieser, A.L. Scholtz and M. Rupp, "Vienna MIMO Testbed", in *EURASIP Journal on Applied Signal Processing*, Volume 2006, Article ID 54868
- [8] V.R. Cadambe and S.A. Jafar, "Interference Alignment and Degrees of Freedom of the K-User Interference Channel", in *IEEE Transactions on Information Theory*, Volume 54, No. 8, August 2008
- [9] C.M. Yetis, T. Gou, S.A. Jafar and A.H. Kayran, "On Feasibility of Interference Alignment in MIMO Interference Networks", in *IEEE Transactions on Signal Processing*, Volume 58, No. 9, September 2010
- [10] J. Balakrishnan, M. Rupp and H. Viswanathan, "Optimal Channel Training for Multiple Antenna Systems", in *Multiaccess, Mobility and Teletraffic for Wireless Communications 5*, 2000
- [11] İ. Emre Telatar, "Capacity of Multi-antenna Gaussian Channels", in *European Transactions on Telecommunications*, Volume 10, Issue 6, 1999